NANO LETTERS

pubs.acs.org/NanoLett

Nanopatterned Metallic Films for Use As Transparent Conductive Electrodes in Optoelectronic Devices

Peter B. Catrysse,* and Shanhui Fan†

Edward L. Ginzton Laboratory and Department of Electrical Engineering, Stanford University, Stanford, California 94305

ABSTRACT We investigate the use of nanopatterned metallic films as transparent conductive electrodes in optoelectronic devices. We find that the physics of nanopatterned electrodes, which are often optically thin metallic films, differs from that of optically thick metallic films. We analyze the optical properties when performing a geometrical transformation that maintains the electrical properties. For one-dimensional patterns of metallic wires, the analysis favors tall and narrow wires. Our design principles remain valid for oblique incidence and readily carry over to two-dimensional patterns.

KEYWORDS Transparent conductive electrodes, nanopatterned metal films, sheet resistance, transmittance, propagating mode, Fano interference, surface resonance.

Transparent conductive electrodes are critical to the operation of optoelectronic devices. Effective electrodes need to combine excellent electrical and optical properties. Transparent conductive metal oxides, such as indium tin oxide (ITO), are commonly used for this purpose. There is, however, substantial interest in replacing them.[1−5] The cost of sputtered metal oxide thin films is relatively high. This prohibits their use in roll-to-roll processed solar cells and large-area organic light-emitting diodes (LEDs) for lighting applications.[6] Metal oxides are also brittle and tend to crack when deposited on flexible substrates, leading to device failure.[7] When used as transparent electrodes on top of organic active layers, the sputtering process causes damage and results in decreased device performance.[8] More fundamentally, however, there is an inherent trade-off between the optical properties (e.g., transmittance) and the electrical properties (e.g., sheet resistance) in this class of electrodes. Thick metal oxide films offer lower sheet resistance, but this comes at the expense of lower optical transmittance.

Recent discoveries regarding the optical properties of nanopatterned metals have opened up an important opportunity to develop a new class of transparent electrodes suitable for optoelectronic devices operating in the visible and near-infrared regime. Nanopatterned metallic films have been shown numerically to possess superior optical transmittance and electrical sheet resistance compared to uniform ITO films.[4] Several experimental reports describe the use of metal grating structures for transparent electrodes.[3,5,9,10] In particular, refs 3 and 5 confirm experimentally that subwavelength metal gratings are good candidates for use as transparent conductive electrodes in organic LEDs and solar cells with performance comparable to that of ITO-based devices.

In this letter, we elucidate the physics governing the performance characteristics of nanopatterned metallic films used as transparent conductive electrodes. By considering both optical and electrical properties, we find that efficient nanopatterned electrodes are often based on optically thin metallic films. The physics observed for these structures is therefore quite different from that of commonly explored nanostructured metallic films that are optically thick.[11−14] Moreover, it is generally insufficient to optimize nanostructured films based upon their optical properties alone, since structural variations will affect the electrical properties as well. Hence, we address the need for simultaneous optical and electrical performance by analyzing nanostructured films that are related by a constant-sheet-resistance transformation. This is a geometrical transformation of the metal film that affects the optical transmittance without modifying the electrical sheet resistance. We identify design principles for one-dimensional (1D) electrode patterns that readily carry over to two-dimensional (2D) patterns. This is significant since there have been no previous reports on numerical studies of the optical and electrical properties of 2D patterns in the context of electrode design.

The general goal in designing transparent conductive electrodes is to achieve high optical transmission without increasing electrical sheet resistance. For transparent conductive electrodes made of uniform metal oxide films, the underlying physics results in a rather simple trade-off between the optical and the electrical properties. An increase in the thickness of the film results in a lower electrical sheet resistance, which improves the electrical performance. It also increases the amount of light absorbed inside film and

* To whom correspondence should be addressed. E-mail: pcatryss@stanford.edu.

† E-mail address: shanhui@stanford.edu.

Received for review: 3/30/2010
Published on Web: 07/22/2010

© 2010 American Chemical Society

DOI: 10.1021/nl1011239 | *Nano Lett.* **2010,** *10,* 2944–2949

BOE v. Samsung IPR2025-01476
Ex-1052

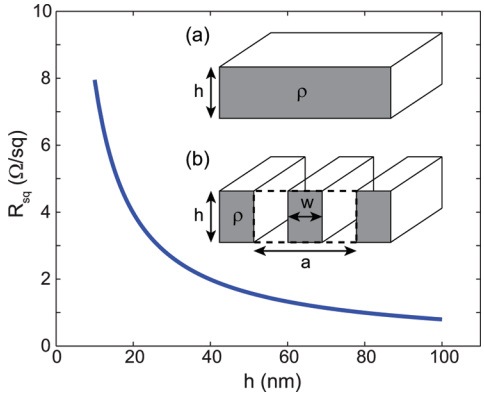

FIGURE 1. Electrical sheet resistance of a metallic film electrode as a function of film thickness. (a) The sheet resistance $R_{sq} = \rho/h$ of a homogeneous film depends on the resistivity of the metal ρ and physical thickness of the film h. (b) The sheet resistance for a nanopatterned film $R_{sq} = (\rho/h)(a/w)$ depends on the one-dimensional (1D) period a and the metal width w as well.

lowers the optical transmittance, which degrades the optical performance. For transparent conductive electrodes that are made of nanopatterned metal films, the physics is more involved and described here.

We start by investigating the optical behavior of nanostructured metal films consisting of a 1D periodic arrangement of metal wires with a rectangular cross-section of subwavelength dimensions. For such geometry, the transverse electric (TE; electric field parallel to the wires) and transverse magnetic (TM; magnetic field parallel to the wires) polarizations can be analyzed independently. The aim of the analysis is to understand the physics that enables high transmission at visible and near-infrared wavelengths in the regime of geometrical parameters that is relevant for transparent electrode design. For concreteness, we focus on wavelengths $\lambda = 400-1000$ nm since most LEDs and photovoltaic cells operate within this range.

The relevant geometrical parameters of nanopatterned electrodes are strongly influenced by the desired electrical properties. In general, the electrical properties of an electrode can be described by its sheet resistance. A uniform metallic film of thickness h and metal resistivity ρ has a sheet resistance $R_{sq} = \rho/h$ expressed in units of Ω/sq (Figure 1, inset a).[15] A nanostructured metallic film with a 1D periodicity a, a wire width w, and a wire thickness h has a sheet resistance $R_{sq} = (\rho/h)(a/w)$ for an electrical current along the wire (Figure 1, inset b). If we use silver with electrical resistivity[16] $\rho_{Ag} = 1.58 \times 10^{-8}$ Ωm to obtain typical values for R_{sq} from 1 to 10 Ω/sq, h ranges from 10 to 100 nm (Figure 1 with $a = 400$ nm and $w = 80$ nm). We observe that metallic electrodes are therefore much thinner than typical metallic films used in many optical studies. Their thickness is in fact comparable to the skin depth of silver in the optical wavelength range. As a result, the physics of such very thin metallic film electrodes can be quite different from that of optically thick metallic films.[17,18]

For a first-principles optical analysis of nanopatterned metallic electrodes, we perform 2D electromagnetic field simulations based on a finite-difference frequency-domain (FDFD) method.[19] FDFD calculates the electromagnetic fields by solving a large sparse linear system derived from Maxwell's equations. This method allows us to use tabulated experimental dielectric constants, including both real and imaginary parts, at every frequency.[16] Plane waves are used as sources and transmitted through the nanopatterned electrode. The Poynting vector (power flux) behind the electrode is measured once with and once without the electrode present. The ratio of the powers defines the transmittance. We perform electromagnetic simulations for both TE and TM polarized plane waves. We set the grid size to 2.5 nm in the transverse direction (along the metallic film) and 5 nm in the longitudinal direction. This enables us to model the very fine features of the field at the metal−air interfaces while maintaining a reasonable size for the simulation domain.

First, we describe the behavior of an optically thick structure consisting of a 1D periodic arrangement of metallic wires. This illustrates the typical regime of operation in optical studies and contrasts it to the behavior of optically thin structures that are the focus of this paper. We choose $a = 400$ nm, which is subwavelength in the regime of interest ($\lambda = 400-1000$ nm) to avoid optical diffraction effects. We further assume $w = 80$ nm and $h = 400$ nm. The thickness h is much larger than the skin depth of metals at optical frequencies (approximately a few tens of nanometers) and a uniform film without patterning is opaque. Figure 2a shows the TE and TM transmittance spectra at visible and near-infrared wavelengths. For TE polarization (solid curve), the spectrum is characterized by a window of high transmission that starts at 400 nm and abruptly ends near 800 nm. On the other hand, for TM polarization (dashed curve) the spectrum exhibits no roll-off. Instead, the transmission becomes quite large and near unity at wavelengths greater than 500 nm. The TM spectrum also features a transmission dip at 400 nm, which is often referred to as a Wood's anomaly.[20] By our choice of periodicity this dip is outside the wavelength range of interest.

We now describe the optical properties of nanopatterned metal films with parameters suitable for electrode design. Figure 2b shows the transmittance spectra for a structure that is identical to the one in Figure 2a, except that h has been reduced to 10 nm. The thickness is now on the order of the skin depth and a homogeneous metallic film becomes translucent. This drastically changes the optical response of a nanopatterned film as well. The TE spectrum (solid curve) no longer exhibits the cutoff behavior that is very prominent in the case of an optically thick film (Figure 2a). Rather, the film becomes almost completely transparent for TE-polarized light, which benefits the intended transparent electrode application. Reducing the thickness has, however, a detrimental impact on the TM spectrum (dashed curve), which

© 2010 American Chemical Society

DOI: 10.1021/nl1011239 | *Nano Lett.* **2010,** *10,* 2944--2949

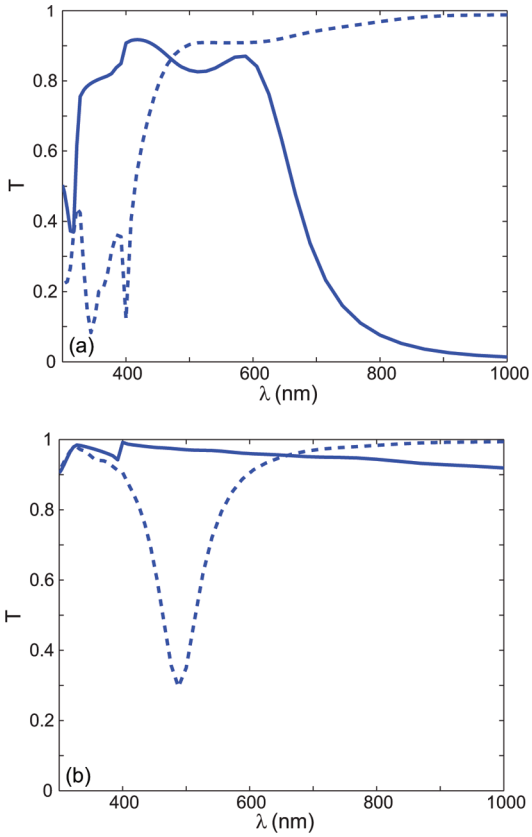

FIGURE 2. Optical properties of 1D nanopatterned silver film electrodes. Transmittance spectra of (a) optically thick films with a = 400 nm, w = 80 nm, and h = 400 nm, and (b) optically thin films with a = 400 nm, w = 80 nm, and h = 10 nm. Solid curves are for TE polarization and dashed curves for TM polarization.

now features a pronounced transmission dip around 500 nm in the middle of the regime of interest.

To understand the transmission behavior observed in Figure 2, we describe the underlying physics in the TE and TM polarization cases. This will allow us to identify strategies for optimizing the optical transmittance of the nanopatterned transparent electrodes.

The physics for TE polarization is dominated by the presence (or absence) of a propagating mode in the gaps between the metal wires. We perform a modal dispersion analysis of an infinitely thick structure with identical period (a = 400 nm) and wire width (w = 80 nm) to confirm this. Figure 3a shows the real (β, upper panel) and imaginary (α, lower panel) part of the complex propagation constant for the fundamental TE_1 mode. The TE_1 mode is propagation-dominant ($\beta > \alpha$) for wavelengths below 750 nm. For wavelengths larger than 750 nm, the mode becomes evanescent ($\beta < \alpha$) and no longer propagates. The behavior of a finite electrode structure can be inferred by comparing the evanescent length ($1/\alpha$) of the mode to the thickness of the film (h). For the optically thick film (dashed curve in lower panel of Figure 3a), the thickness (400 nm) exceeds the evanescent length in the wavelength range above 800 nm. The structure thus exhibits strong cutoff behavior around 800 nm, as is confirmed in the transmittance spectrum of Figure 2a (solid curve). In contrast, the thickness of the optically thin film (10 nm, outside the range graphed in lower panel of Figure 3a) is much smaller than the evanescent length over the entire wavelength range from 400 to 1000 nm. No distinct cutoff behavior should therefore be observed in consistency with the spectrum of Figure 2b (solid curve).

The physics for TM polarization is governed by the interference between two possible transmission mechanisms. First, the structure supports propagating modes inside the gaps at all wavelengths. For wavelengths larger than the periodicity, in particular, the structure supports the fundamental TM_0 mode with transverse electromagnetic (TEM)-like behavior. The presence of a propagating mode, by itself, should lead to broadband transmission through the structure. Second, the top and bottom metal-dielectric surfaces of the structures support TM surface modes as well. These are often referred to as surface plasmon polariton (SPP) modes.[21] On the metal−air interface of a uniform film, light does not couple to SPP modes; the SPP wave vector ($\mathbf{k}_{SPP}$) is larger than the free-space parallel wave vector ($k_0 \sin\theta$, where $k_0 = 2\pi/\lambda$ and θ is the angle of incidence). The periodicity of the structure provides the wave vector of the incident light with additional momentum ($G = 2\pi/a$). This allows SPP modes to couple to the incident light at discrete spectral locations ($\mathbf{k}_{SPP} = k_0 \sin\theta \pm m\,G$, where m is a positive integer) and creates resonances with narrow spectral features. Fano-type interference between the propagating TEM-like mode in the gaps (that provides a direct pathway), and the SPP resonant modes on the surface (that provide an indirect pathway), dominates the TM transmission characteristics.[22]

In the case of a thick film (a = 400 nm, w = 80 nm, h = 400 nm), the broad window of high transmission for wavelengths larger than 400 nm is closely related to the excitation of the propagating TEM-like mode, as seen in the right-most inset of Figure 3b with the magnetic field profile Re (H_z) at λ = 800 nm. The dip at 400 nm, on the other hand, is related to the resonant excitation of SPP modes. Figure 3b (main panel) shows the magnetic field intensity spectrum, measured at a point near the metal-dielectric interface. It features a narrow resonance peak centered at 400 nm (magnetic field profile Re (H_z) shown in the left-most inset). This peak is associated with the two weakly coupled SPP modes supported by the top and bottom interfaces of the thick film. Its location matches very well with the location of the dip in the spectrum of a typical wire-grid or hole array structure made from an optically thick film (Figure 2a). The presence of a dip in the transmission spectrum resulting from the resonant excitation of a surface wave is often referred to as a resonant Wood's anomaly.[20,23] Since it occurs at the edge of the spectrum of interest, it does not significantly affect the high transmission behavior enabled by the propagating TEM-like mode.

© 2010 American Chemical Society

DOI: 10.1021/nl1011239 | Nano Lett. 2010, 10, 2944--2949

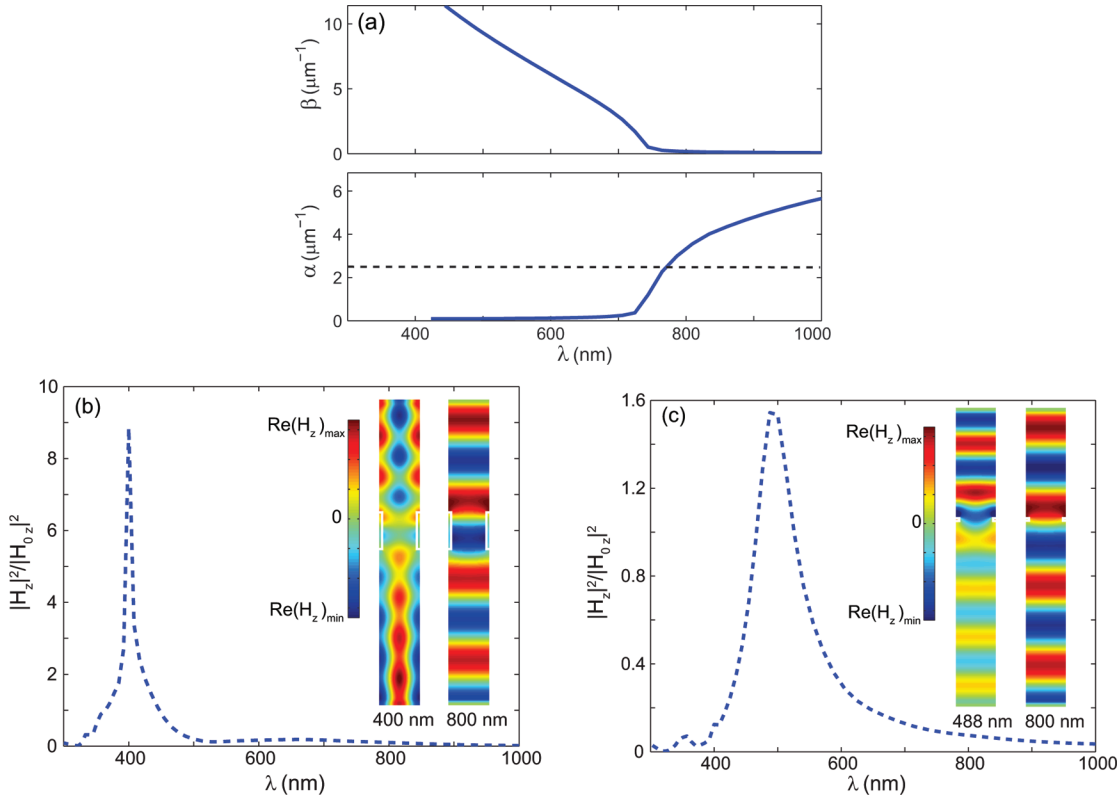

FIGURE 3. Propagating modes and surface resonances supported by 1D nanopatterned silver film electrodes. (a) Real and imaginary part of the complex propagation constant for the TE_1 mode supported by an infinitely long ($h = \infty$) structure with $a = 400$ nm and $w = 80$ nm. The dashed horizontal line in the lower panel corresponds to the thickness of a 400 nm thick film. (b,c) Normalized magnetic field intensity spectrum for TM polarization measured 5 nm above the air−metal interface for (b) a thick film structure with $a = 400$ nm, $w = 80$ nm, and $h = 400$ nm, and (c) a thin film structure with $a = 400$ nm, $w = 80$ nm, and $h = 10$ nm. Insets show the real part of the magnetic field profile for (b) at $\lambda = 400$ and 800 nm and for (c) at $\lambda = 488$ and 800 nm, respectively.

For the thin film ($a = 400$ nm, $w = 80$ nm, $h = 10$ nm), Figure 3c shows the magnetic field intensity spectrum measured at the metal-dielectric surface. The resonance is centered at 488 nm. For a thin-film structure, the single-interface SPP modes couple and the resonance is red shifted in comparison to the thick-film surface resonance. The thinner the film is, the stronger the coupling becomes, and the larger the red shift is. The wavelength of the resonance is in excellent agreement with the location of the dip in the transmission spectrum of the electrode structure. Since the surface modes on thin films exhibit a relatively flat (slow-light) dispersion behavior, the location of this dip can not be removed from the regime of interest by simply reducing the periodicity. The presence of two physical mechanisms in the range of interest, that is, a direct pathway (propagating TEM-like mode) and a resonant pathway (coupled SPP resonance), therefore leads to Fano-type interference.[24,25] This interference is destructive (magnetic field profile Re (H_z) at $\lambda = 488$ nm shown in the left-most inset of Figure 3c) and results in a transmission dip. For optically thin electrode structures, this has an important impact on the transmission in the regime of interest.

We now turn to the optimization of nanostructured films for use as transparent conductive electrodes. First, we observe that sheet resistance for 1D nanostructured metallic films made of the same metal is constant when the cross-sectional metal area wh is fixed (within one period a). Hence, we define a geometrical transformation that maintains the cross-sectional area per period $h_1w_1/a = h_2w_2/a = h_3w_3/a$ (Figure 4 inset). This constant-sheet-resistance transformation establishes a class of electrodes with identical electrical properties (sheet resistance). Once the electrical properties are fixed, we can find the parameters that optimize the optical properties for a given class of electrodes. This addresses the need for simultaneous optical and electrical performance.

In what follows, we investigate three classes of electrodes with constant sheet resistance $R_{sq} = 3.2\Omega$/sq, $R_{sq} = 1.6\Omega$/sq, and $R_{sq} = 0.8\Omega$/sq, respectively. In Figure 4, we show the transmittance, averaged for TM and TE polarization over all wavelengths from 400 to 1000 nm, as we vary the metal wire width w. While the sheet resistance is kept constant by the transformation, the optical transmittance varies greatly.

The curves in Figure 4 show a clear trend for the optical behavior as a function of w. For a constant sheet resistance, the optimal structures with near-complete transmittance are those with small w and large h. This trend is consistent with the physics discussions we presented above. The values of

© 2010 American Chemical Society

DOI: 10.1021/nl1011239 | Nano Lett. 2010, 10, 2944--2949

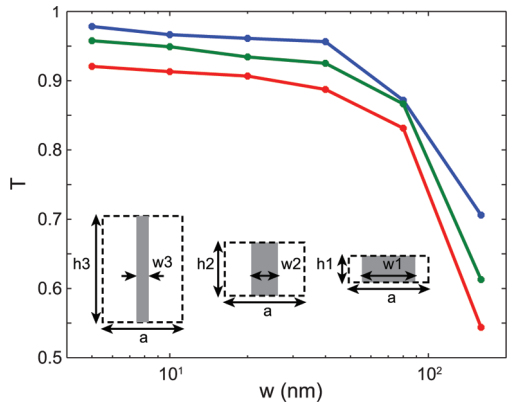

FIGURE 4. Optical transmittance of 1D nanopatterned silver film electrodes. The transmittance at normal incidence is graphed versus wire width for electrodes with sheet resistance $R_{sq} = 3.2\Omega$/sq (blue curve), $R_{sq} = 1.6\Omega$/sq (green curve), and $R_{sq} = 0.8\Omega$/sq (red curve), respectively. The transmittance in the main panel is the average for TM and TE polarization over all wavelengths from 400 to 1000 nm. Inset shows how the sheet resistance of 1D nanopatterned films is maintained by an area-conserving geometrical transformation, $h_1w_1/a = h_2w_2/a = h_3w_3/a$.

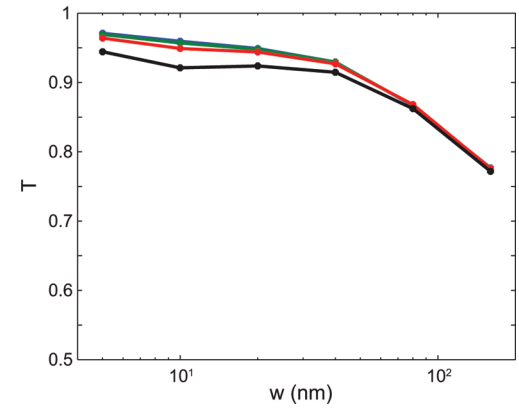

FIGURE 5. Optical transmittance of 1D nanopatterned silver film electrodes for oblique incidence. Transmittance is graphed versus wire width for a sheet resistance of $R_{sq} = 3.2\Omega$/sq. Blue, green, red, and black curves show the average transmittance (for TM and TE polarization over all wavelengths from 400 to 1000 nm) for 0, 5, 10, and 20°, respectively.

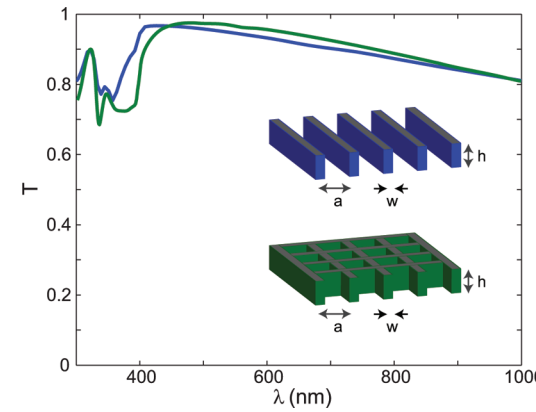

FIGURE 6. Optical properties of two-dimensional (2D) nanopatterned silver film electrodes. Transmittance spectra are shown for 1D and 2D periodic nanopatterned electrodes with a sheet resistance of $R_{sq} = 1.6\Omega$/sq (inset shows pattern geometry with period $a = 400$ nm, metal wire width $w = 40$ nm, and film thickness $h = 100$ nm). The blue curve is obtained by averaging TE and TM polarization results for the 1D pattern.

the transmission spectra for TM polarization are high because the SPP modes remain largely uncoupled when h is large. The transmission spectra values for TE polarization are also high because the cutoff wavelength is pushed toward longer wavelengths when w is small. In contrast, the average transmission is low for large w and small h. The behavior in this limit is primarily due to the deterioration of the TM transmission resulting from the resonant dip associated with coupled SPP modes. Transmission for TE polarization, on the other hand, remains relatively high despite a cutoff at shorter wavelength because h is small.

Within a class of electrodes defined by the constant-sheet-resistance transformation, the optical analysis reveals a wide transmittance optimum for nanostructured metallic films with narrow ($w < 40$ nm, less than 10% metal fill-factor) and tall wires. For example, transmittance of electrodes with $R_{sq} = 1.6\Omega$/sq remains approximately constant at around 95% for $w = 5-40$ nm (Figure 4). The optimal design of these structures is therefore rather robust with respect to parameter variations.

The design guidelines that we have identified so far are immediately applicable to electrodes that receive or emit near-normal light. They apply, for example, to photovoltaic cells that track the sun. For nontracking cells or other devices that require a wider acceptance cone of light, we now analyze the off-axis behavior (obliquely incident light). Figure 5 shows the transmittance for an electrode with sheet resistance $R_{sq} = 3.2\Omega$/sq for light at 0 (blue), 5 (green), 10 (red), and 20° (black) angle of incidence. The off-axis behavior for the nanopatterned electrode qualitative follows the on-axis behavior quite well. This is true even for relatively large angles. It confirms that the design guidelines as described here are relatively robust and apply to a wider acceptance cone of light as well. (For solar concentration, a 20° angle of incidence corresponds to more than 2000 suns. Thus our results should be quite applicable even for high concentration photovoltaic systems.)

Many of the design principles that we have identified for 1D nanopatterned electrodes also readily carry over to 2D patterns. We note that 2D patterns have not been previously explored in the context of transparent electrode design. As an example, we consider a 2D (green curve) nanopatterned silver film with a sheet resistance $R_{sq} = 1.6\Omega$/sq (Figure 6). The geometry has a periodicity $a = 400$ nm, a metal wire width $w = 40$ nm, and a film thickness $h = 100$ nm. The transmission spectrum is approximately flat over the entire wavelength range of interest (Figure 6, green curve).

The transmission spectrum for such a 2D patterned structure in fact matches quite well with the polarization-averaged transmission spectrum (Figure 6, blue curve) of a corresponding 1D patterned structure with the same sheet

© 2010 American Chemical Society

DOI: 10.1021/nl1011239 | Nano Lett. 2010, 10, 2944--2949

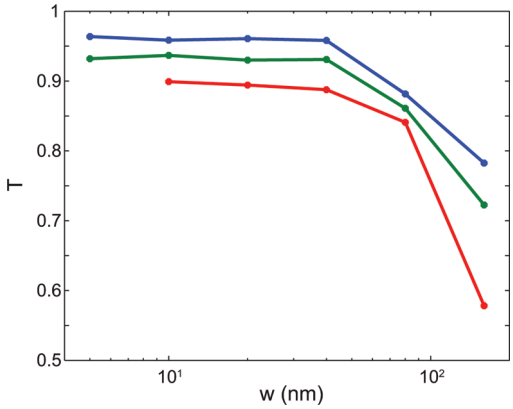

FIGURE 7. Optical transmittance of 2D nanopatterned silver film electrodes. Transmittance is graphed versus wire width for constant sheet resistance. The blue, green, and red curves show the average transmittance (for TM and TE polarization over all wavelengths from 400 to 1000 nm) for a sheet resistance of $R_{sq} = 3.2\Omega$/sq, $R_{sq} = 1.6\Omega$/sq, and $R_{sq} = 0.8\Omega$/sq, respectively.

resistance (Figure 6, inset). The 2D pattern can be seen here as a combination of two 1D patterns that are rotated 90° with respect to each other. Hence, we can think of transmittance through the 2D pattern as the average of the TE and TM transmittances through a 1D pattern. The excellent qualitative agreement in transmittance suggests that the behavior of 1D nanopatterned electrodes can be used to predict the optical transmittance behavior of 2D nanopatterned electrodes.

Figure 7 shows optical transmittance of 2D nanopatterned silver film electrodes versus wire width for constant sheet resistance. The blue, green, and red curves show the average transmittance (for TE and TM polarization over all wavelengths $\lambda = 400-1000$ nm) for $R_{sq} = 3.2\Omega$/sq, $R_{sq} = 1.6\Omega$/sq, and $R_{sq} = 0.8\Omega$/sq, respectively. The behavior of the 2D structures is quite similar to that of the 1D structures and the same design guidelines that we presented for 1D structures can thus be extended to 2D structures.

In summary, we find that the optical behavior of 1D nanopatterned electrodes can be understood in terms of the propagating modes (TE and TM) and resonances associated with SPP modes (TM). When the propagating modes are the only pathway, they enable high transmission (TE). When they form a direct pathway in combination with a resonant indirect pathway (TM), interference can significantly affect transmittance. For electrodes based on periodically patterned metal films, the constant-sheet-resistance transformation leads to designs based on narrow and tall wires. Such designs allow large optical transmittance over the entire visible and near-infrared range for both TE and TM polarization. Finally, our design principles remain valid for oblique incidence and readily carry over to 2D patterns.

Acknowledgment. The authors thank J.-Y. Lee and P. Peumans for bringing this problem to their attention. This work was supported by the Center for Advanced Molecular Photovoltaics (CAMP) under Award No. KUSC1-015-21 made by the King Abdullah University of Science and Technology, and by DOE Grant DE-FG02-07ER46426. The computation is performed through the support of NSF-LRAC program.

REFERENCES AND NOTES

(1) Wu, Z. C.; Chen, Z. H.; Du, X.; Logan, J. M.; Sippel, J.; Nikolou, M.; Kamaras, K.; Reynolds, J. R.; Tanner, D. B.; Hebard, A. F.; Rinzler, A. G. *Science* **2004**, *305*, 1273–1276.
(2) Zhang, M.; Fang, S. L.; Zakhidov, A. A.; Lee, S. B.; Aliev, A. E.; Williams, C. D.; Atkinson, K. R.; Baughman, R. H. *Science* **2005**, *309*, 1215–1219.
(3) Kang, M. G.; Guo, L. J. *Adv. Mater.* **2007**, *19*, 1391–1396.
(4) Lee, J. Y.; Connor, S. T.; Cui, Y.; Peumans, P. *Nano Lett.* **2008**, *8*, 689–692.
(5) Kang, M. G.; Kim, M. S.; Kim, J. S.; Guo, L. J. *Adv. Mater.* **2008**, *20*, 4408–4413.
(6) Forrest, S. R. *Nature* **2004**, *428*, 911–918.
(7) Chen, Z.; Cotterell, B.; Wang, W.; Guenther, E.; Chua, S. J. *Thin Solid Films* **2001**, *394*, 202–206.
(8) Kim, H. K.; Kim, D. G.; Lee, K. S.; Huh, M. S.; Jeong, S. H.; Kim, K. I.; Seong, T. Y. *Appl. Phys. Lett.* **2005**, *86*, 183503.
(9) Aernouts, T.; Vanlaeke, P.; Geens, W.; Poortmans, J.; Heremans, P.; Borghs, S.; Mertens, R.; Andriessen, R.; Leenders, L. *Thin Solid Films* **2004**, *451*, 22–25.
(10) Tvingstedt, K.; Inganas, O. *Adv. Mater.* **2007**, *19*, 2893–2897.
(11) Tamada, H.; Doumuki, T.; Yamaguchi, T.; Matsumoto, S. *Opt. Lett.* **1997**, *22*, 419–421.
(12) Ebbesen, T. W.; Lezec, H. J.; Ghaemi, H. F.; Thio, T.; Wolff, P. A. *Nature* **1998**, *391*, 667–669.
(13) Catrysse, P. B.; Suh, W. J.; Fan, S. H.; Peeters, M. *Opt. Lett.* **2004**, *29*, 974–976.
(14) Verslegers, L.; Catrysse, P. B.; Yu, Z. F.; White, J. S.; Barnard, E. S.; Brongersma, M. L.; Fan, S. H. *Nano Lett.* **2009**, *9*, 235–238.
(15) Muller, R. S.; Kamins, T. I.; Chan, M. *Device electronics for integrated circuits*, 3rd ed.; John Wiley & Sons: New York, 2003.
(16) Lide, D. R. *CRC Handbook of Chemistry and Physics*, 90th ed.; CRC Press: Boca Raton, Fl, 2009.
(17) Braun, J.; Gompf, B.; Kobiela, G.; Dressel, M. *Phys. Rev. Lett.* **2009**, *103*, 203901.
(18) Rodrigo, S. G.; Martin-Moreno, L.; Nikitin, A. Y.; Kats, A. V.; Spevak, I. S.; Garcia-Vidal, F. J. *Opt. Lett.* **2009**, *34*, 4–6.
(19) Veronis, G.; Fan, S. Overview of Simulation Techniques for Plasmonic Devices. In *Surface plasmon nanophotonics*; Brongersma, M. L., Kik, P., Eds.; Springer: New York, 2007.
(20) Hessel, A.; Oliner, A. A. *Appl. Opt.* **1965**, *4*, 1275–1297.
(21) Maier, S. A. *Plasmonics: fundamentals and applications*; Springer: New York, 2007.
(22) Fano, U. *Phys. Rev.* **1961**, *124*, 1866–1878.
(23) Sarrazin, M.; Vigneron, J. P.; Vigoureux, J. M. *Phys. Rev. B* **2003**, *67*, 85415.
(24) Fan, S. H.; Suh, W.; Joannopoulos, J. D. *J. Opt. Soc. Am. A* **2003**, *20*, 569–572.
(25) Catrysse, P. B.; Fan, S. H. *J. Nanophotonics* **2008**, *2*, 021790.

© 2010 American Chemical Society

DOI: 10.1021/nl1011239 | *Nano Lett.* **2010,** *10,* 2944--2949